Inorganic Chemistry

Article

pubs.acs.org/IC

A Combined Computational and Spectroelectrochemical Study of Platinum-Bridged Bis-Triarylamine Systems

Matthias Parthey,[†] Kevin B. Vincent,[‡] Manuel Renz,[†] Phil A. Schauer,[‡] Dmitry S. Yufit,[‡] Judith A. K. Howard,[‡] Martin Kaupp,*[,†] and Paul J. Low*[,‡,§]

[†]Institut für Chemie, Theoretische Chemie, Technische Universität Berlin, Sekretariate C7, Straße des 17. Juni 135, 10623 Berlin, Germany

[‡]Department of Chemistry, Durham University, South Road, Durham DH1 3LE, United Kingdom

[§]School of Chemistry and Biochemistry, University of Western Australia, Crawley, Perth, WA 6009, Australia

Supporting Information

ABSTRACT: The character of the electronic transitions in the ultraviolet−visible−near infrared (UV−vis−NIR) spectra of platinum-bis(alkynyl) bridged, bis-triarylamine mixed-valence systems *trans*-$[Pt(C{\equiv}CC_6H_4NAr_2)_2(PR_3)_2]^{n+}$ (R = ethyl, Ar = $C_6H_4CH_3$-4 (**1**) or $C_6H_4OCH_3$-4 (**2**); R = Ph, Ar = $C_6H_4CH_3$-4 (**3**) or $C_6H_4OCH_3$-4 (**4**), *n* = 0, 1, 2) has been determined from a combination of spectroscopic measurement and density functional theory calculations. The hybrid functional BLYP35 in combination with a suitable solvent model (i.e., conductor-like screening model (COSMO)) has been used to model the UV−vis−NIR and IR spectroscopic properties of $[\mathbf{1}-\mathbf{4}]^+$, to confirm the description of $[\mathbf{1}-\mathbf{4}]^+$ as examples of metal-bridged organic mixed-valence compounds, and to assign the principal features of the electronic spectra, including the triarylamine-based intervalence charge transfer transition located in the NIR region. The successful modeling of the charge distribution within the system demonstrates the utility of the BLYP35-COSMO protocol as a tool for use in the study of intramolecular charge transfer properties in mixed-valence complexes.

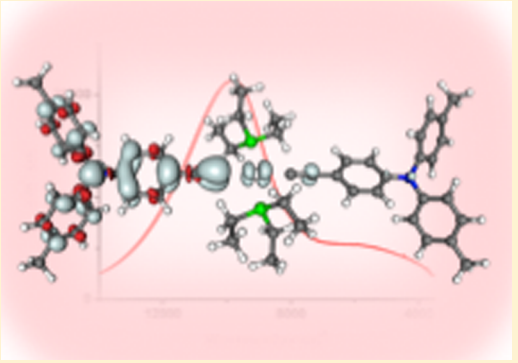

INTRODUCTION

The study of redox-active systems that exhibit facile intramolecular electron transfer (ET) processes continues to attract attention due to potential applications in electrochromic devices[1] and as components in future molecular electronics technology.[2] Mixed-valence (MV) complexes represent perhaps the most widely exploited test beds for such studies, due in no small part to the models developed by Hush and others that link experimentally observable spectroscopic parameters to underlying details of electronic coupling between the remote sites.[3−5] While the great majority of MV molecular compounds feature metal-complex electrophores and conjugated organic bridging ligands[6−10] borrowing from the designs established by the Creutz-Taube ion,[11,12] there is a growing interest in organic MV compounds, in which nonmetal-based electrophores serve as the sites for redox reactions.[13] The combination of these concepts has led to a small number of "inverted" MV complexes being designed, in which organic redox systems are bridged by a metal-based complex.[14−19] In turn, these complexes serve as models to study the transmission of electronic effects through metal complex-based bridges.[20−26]

Regardless of the constituents and composition of the system, electronic absorption data are crucial to the characterization of MV complexes.[4,27] While there is a wealth of information contained in the (often overlooked) metal−ligand charge transfer (MLCT)/ligand−metal charge transfer (LMCT) transitions that usually fall in the visible region of the spectrum,[4,28−30] the lower-energy intervalence charge transfer (IVCT) band typically found in the near infrared (NIR) region is usually the primary source of information concerning the electronic character of a MV system.[3−5,27,31] The experimental bandwidth at half height of the NIR band envelope is often used as the main criterion to classify MV systems following the Robin-Day scheme[32] by comparison with the bandwidth for weakly coupled systems calculated from the Hush model.[33] However, the observation of a simple, Gaussian-shaped IVCT band is rare in organometallic MV systems,[34,35] and more often the near-degeneracy of the d orbitals leads to a set of transitions close in energy and thus to a series of overlapping NIR bands.[5] Although typically complicated by solvent-induced band broadening, excitation energies and bandwidth are often extracted from the experimental spectral envelopes by Gaussian deconvolution. However, a unique analytical solution to the deconvolution is often not possible, leaving considerable ambiguity in the spectroscopic assignments and much space for individual interpretation. Various fits of near-equivalent quality can be obtained by varying the number, width, and/or position of the

Received: October 8, 2013
Published: January 22, 2014

   dx.doi.org/10.1021/ic402538e | *Inorg. Chem.* 2014, 53, 1544−1554

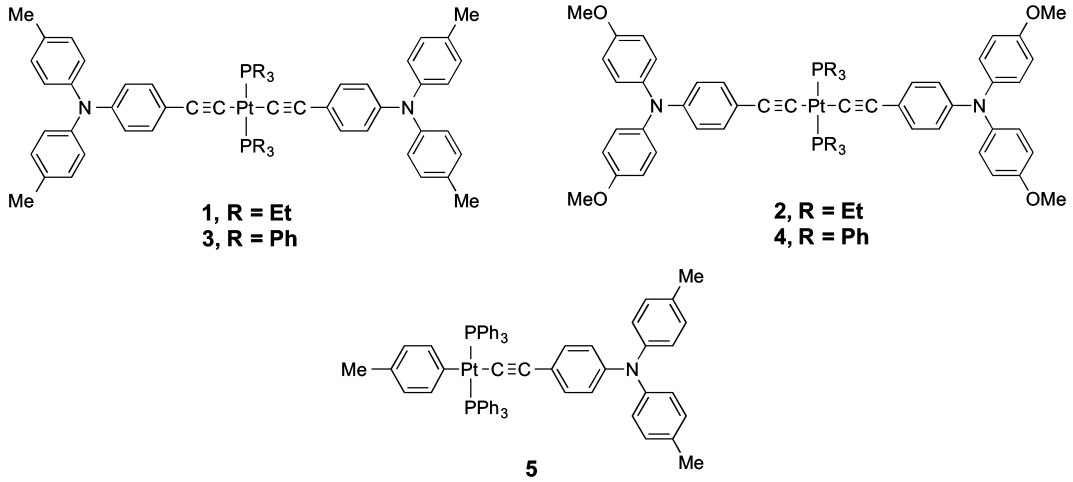

Figure 1. Compounds studied in this work.

Gaussian-shaped sub-bands used to model the NIR band envelope. Another complication to Gaussian-based deconvolutions and spectral fitting occurs in strongly coupled systems, which often exhibit bands with a pronounced "cutoff" on the low-energy side of the band, leading to an asymmetric shape of the NIR band,[4,13] making the Gaussian shape of sub-bands an invalid approximation. Considering these fundamental difficulties in analytical treatment of the spectroscopic band envelopes, a quantum-chemical perspective is highly desirable.[36,37]

To achieve a proper description of the electron-transfer transitions, it is important to account for effects from both dynamic and nondynamic correlation, keeping in mind that there is no clear-cut separation between these extremes. With large configuration−interaction or coupled-cluster calculations within an ab initio framework this problem could, in principle, be addressed. Unfortunately, because of the size of typical MV systems those methods are computationally too demanding. Hartree−Fock calculations generally give solutions that are biased toward localized descriptions, and standard density functional theory (DFT) calculations generally overemphasize the delocalized descriptions. In addition, almost all experimental data are obtained in a polar solvent environment, which inevitably stabilizes a localized charge-separated situation, raising further challenges for the computational models, which must also account for the effects of solvation on the relative stability of different electronic states. On the basis of extensive benchmarking, originally for the ground- and excited-state properties of bis-triarylamine radical cations containing two *N*,*N*-di(4-anisyl)-moieties as redox centers bridged by various organic units,[36,37] later also for transition-metal complexes,[38] a quantum-chemical protocol[36] has recently been developed. It employs the BLYP35 (global) hybrid functional with 35% exact exchange, together with continuum-solvent models, and it has been shown to give a near-optimum compromise for both class II and class III systems. While the protocol tends to underestimate transition energies for localized (Class II) systems and modestly overestimates them for molecules exhibiting delocalized (Class III) behavior, the time-dependent DFT (TDDFT) results may be considered in reasonable agreement with experimental UV−vis−NIR data (the different treatment of nonequilibrium solvation may lead to somewhat different results for various program implementations).

A previous report by Jones et al. has shown that the closely related platinum-bis(alkynyl) bridged bis-triarylamine compound *trans*-[Pt{C≡CC_6H_4N ($C_6H_4OCH_3$-4)$_2$}$_2$(PEt_3)$_2$] (Et = ethyl) undergoes amine-centered oxidations, giving rise to an unusual metal-bridged organic MV compound, the Pt center serving to limit extensive delocalization of the radical and engineering Class II MV character in the one-electron oxidized species.[15] In this earlier work, TDDFT calculations (B3LYP/LANL2DZ) were performed on the crystallographically determined structure of *trans*-[Pt{C≡CC_6H_4N ($C_6H_4OCH_3$-4)$_2$}$_2$(PEt_3)$_2$] to support the spectroscopic observations made on the family of neutral, mono-, and dicationic complexes, the latter two being obtained by stoichiometric chemical oxidation. The key localized orbitals thought to be involved in the IVCT transition in the MV monocation were derived from a linear combination of the HOMO and HOMO−1 of the neutral compound following from a Koopmans' Theorem-based treatment of the electronic coupling. As a step toward the ultimate goal of achieving general and universal quantum-chemical protocols for describing and understanding intramolecular charge transfer (CT) events, we report here a combined experimental and computational study of the spectroscopic properties of the family of platinum-bis(alkynyl) bridged bis-triarylamine complexes *trans*-[Pt(C≡$CC_6H_4NAr_2$)$_2$ (PR_3)$_2$]$^{n+}$ (R = Et or Ph, Ar = $C_6H_4CH_3$-4 or $C_6H_4OCH_3$-4, **1**−**4**; *n* = 0, 1, 2) and the model monoamine complex *trans*-[Pt{C≡CC_6H_4N (C_6H_4Me-4)$_2$} ($C_6H_4CH_3$-4)(PPh_3)$_2$] (**5**).

RESULTS AND DISCUSSION

Syntheses and Characterization. Compounds **1**−**5** (Figure 1) were synthesized via CuI-catalyzed dehydrohalogenation reactions of *trans*-$PtCl_2(PEt_3)_2$, *cis*-$PtCl_2(PPh_3)_2$, or *trans*-$PtI(C_6H_4Me$-4) (PPh_3)$_2$ and the corresponding ethynyl-substituted triarylamine.[15,39] The compounds were isolated in good yield after purification by preparative thin-layer chromatography (silica), with all details provided in the Supporting Information.

Compounds **1**−**5** are each characterized with a single ν(C≡C) absorption near 2100 cm^{-1}. Matrix-assisted laser desorption ionization or atmospheric solids analysis probe (ASAP) mass spectrometry (MS) for compounds **1**−**4** gave signals corresponding to the [M]$^+$ or [M + H]$^+$ molecular ions, while ASAP MS for compound **5** contained [Pt(C_6H_4Me)(PPh_3)$_2$ + H]$^+$ as the highest molecular mass fragment. The $^{31}P\{^1H\}$ NMR spectrum for each compound shows a singlet resonance with platinum satellites: **1** 11.0 (s, $^1J_{P-Pt}$ = 2385 Hz); **2** 9.93 (s, $^1J_{P-Pt}$ = 2373 Hz); **3** 18.73 (s, $^1J_{P-Pt}$ = 2663 Hz); **4** 17.69,

dx.doi.org/10.1021/ic402538e | Inorg. Chem. 2014, 53, 1544−1554

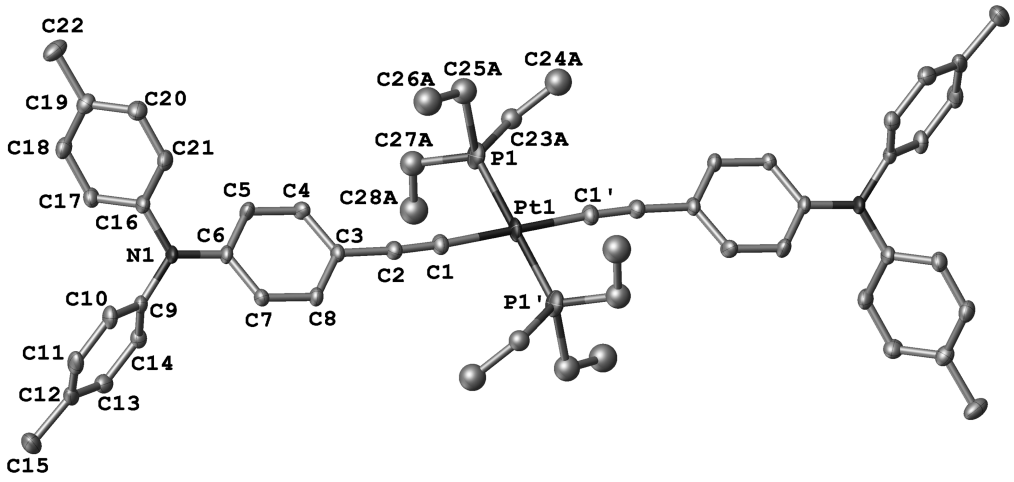

Figure 2. A plot of a molecule of compound **1** showing the atom-labeling scheme, with thermal ellipsoids plotted at 50%. The atom Pt1 is located in a special position on a center of symmetry. Hydrogen atoms have been omitted, and only one component of a disordered ethyl chain is shown for clarity. Selected bond lengths (Å) and angles (deg): Pt1−P1 2.2667(19); Pt1−C1 1.999(6); C1−C2 1.194(8); C2−C3 1.453(8); N1−C6 1.423(7); N1−C9 1.423(7); N1−C16 1.409(8); Pt1−C1−C2 175.9(6); C1−C2−C3 178.5(7); C1−Pt1−P1 87.82(18); C1′−Pt1−P1 92.17(18).

(s, $^1J_{P-Pt}$ = 2671 Hz); **5** 20.25 (s, $^1J_{P-Pt}$ = 3003 Hz). The $^{13}C\{^1H\}$ NMR spectra of compounds **1**, **2**, and **4** show characteristic resonances for alkynyl carbons at 109.05 and 106.13 (**1**), 108.90 and 105.40 (**2**), and 113.11 and 108.81 (**4**). However, due to poor solubility not all of the quaternary carbons of **3** or **5** could be observed.

Crystals of compound **1** were grown by slow diffusion of EtOH into a CH_2Cl_2 solution of the complex to give pale yellow needles that were suitable for X-ray diffraction (Figure 2). The molecule is located in the inversion center and therefore has trans-configuration of the ligands. The coordination geometry at the platinum center is square planar. The extended rigid rod structure is evidenced by the approximately linear C3−C2−C1−Pt1− C1′−C2′−C3′ chain (Figure 2). The structure also shows the characteristic propeller arrangement of the phenyl moieties and the trigonal planar nitrogen geometry associated with the triarylamine moiety.[40−42] The bond lengths and angles are common with the other known examples of *trans*-$Pt(PR_3)_2$ bis(acetylide) systems,[43−48] such as *trans*-$[Pt\{C{\equiv}CC_6H_4N(C_6H_4OMe\text{-}4)_2\}_2(PEt_3)_2]$ (**2**)[15] and *trans*-$[Pt\{C{\equiv}CC_6H_4NPh_2\}_2(PBu_3)_2]$.[49]

(Spectro)Electrochemical Investigations. Electrochemical methods are potentially useful tools with which to assess the electronic interactions between two or more redox-active entities mediated by a common bridging ligand, although the extraction of electronic information from the myriad of medium effects is not possible without considerable attention to detail and often requires comparisons of data from a series of closely related complexes.[6,7,50−53] Nevertheless, electrochemical measurements provide a simple method for the determination of comproportionation constants and hence of the thermodynamic stability of individual redox states with respect to disproportionation.[54] Bis-triarylamine compounds featuring various π-conjugated organic- and organometallic-based bridges have been shown to exhibit two reversible, one-electron oxidation processes centered on the amine cores,[40−42,55] with the separation of these processes often large enough to permit study of the organic MV species.[13,15] In line with these general trends, the cyclic voltammograms of the bis(alkynyl)platinum-bridged compounds **1**−**4** each exhibit two reversible triarylamine-localized one-electron redox processes (Table 1). The moderate degree of separation (ΔE) between the amine-based oxidation processes in each of the compounds **1**−**4** in NBu_4PF_6, measured by both cyclic and differential-pulse voltammetry, gives rise to small comproportionation constants, K_c of 10−160 (Table 1). However, these values are consistent in both 0.1 M NBu_4PF_6 and the "Geiger electrolyte" 0.1 M $NBu_4[B\{C_6H_3\text{-}3,5\text{-}(CF_3)_2\}_4]$, which features the very weakly coordinating $[B\{C_6H_3\text{-}3,5\text{-}(CF_3)_2\}_4]^-$ ($[BAr^F{}_4]^-$) anion.[52,53] Given the likely similar energies of solvation, ion pairing, and electronic factors across the series of complexes in Table 1, the moderate ΔE values offered by compounds **1**−**4** are consistent with a modest degree of through-bond electronic interaction between the amine centers.[7] This suggestion is also in agreement with arguments presented earlier based on the observation of a low-energy IVCT band in $[\mathbf{2}]^+$.[15] In contrast, the monoamine compound **5** exhibits a single reversible amine-centered oxidation due to the presence of a single redox-active amine moiety.

Spectroscopic data permit a more detailed assessment of the physical and electronic structures of the redox products than electrochemical measurements used in isolation. While the UV−

Table 1. Oxidation Potentials for Platinum Complexes 1−5 and Related Organic Bis-Triarylamines[a]

compound	$[X]^-$	E_1/V	E_2/V	ΔE/V	K_c
$\{C_2C_6H_4N(C_6H_4OMe\text{-}4)_2\}_2$[55]	$[PF_6]^-$	0.29	0.39	0.10	50
$[C_6H_4\{C_2C_6H_4N(C_6H_4OMe\text{-}4)_2\}_2]$[55]	$[PF_6]^-$	0.28	0.34	0.06	10
1	$[PF_6]^-$	0.27	0.40	0.13	160
	$[BAr^F{}_4]^-$	0.25	0.39	0.14	
2	$[PF_6]^-$	0.17	0.23	0.06	10
	$[BAr^F{}_4]^-$	0.20	0.26	0.06	
3	$[PF_6]^-$	0.24	0.36	0.12	108
	$[BAr^F{}_4]^-$	0.25	0.36	0.11	
4	$[PF_6]^-$	0.21	0.27	0.06	10
	$[BAr^F{}_4]^-$	0.22	0.29	0.07	
5	$[PF_6]^-$	0.37			

[a] CV in CH_2Cl_2 with 0.1 M $NBu_4[X]$ at a scan rate of 100 mV/s and referenced against DMFc at −0.48 V vs FcH (FcH = +0.0 V). Peaks for the Pt complexes were resolved using differential pulse voltammetry.

dx.doi.org/10.1021/ic402538e | Inorg. Chem. 2014, 53, 1544−1554

vis−NIR spectrum of $[2]^+$ has been determined from samples prepared by chemical oxidation of **2**,[15] spectroscopic information for the series $[1-4]^{n+}$ was conveniently obtained here using spectroelectrochemical methods.[56] The IR spectra of the neutral complexes **1**−**4** are characterized by a single weak ν(C≡C) band (Table 2), consistent with the highly symmetric distribution of electron density over the molecular backbone (Figure 3). On oxidation, the IR band profile evolves through a unique ν(C≡C) band pattern associated with the comproportionated equilibrium mixture of the neutral, monocationic, and dicationic states to a strong absorption feature characteristic of the dicationic state (Figure 3). The observation of multiple ν(C≡C) bands associated with the monocation, perhaps due to the effects of Fermi coupling,[57] in combination with the low comproportionation constant, which ensures solutions of the monocations also contain appreciable amounts of the neutral and dicationic forms, makes definitive assignment of the individual vibrational modes associated with the monocationic state difficult. The assignment is assisted, however, as the unique features of the IR spectra associated with the monocationic states are coupled with a rise and fall in a unique low-energy (NIR) electronic absorption band near 5000 cm^{-1} (the character of which is discussed in more detail below). The observation of IR spectral band profiles for the mono-oxidized complexes $[1-4]^+$, which resemble a superposition of the spectra of the associated neutral and dicationic forms, suggests a description of these species in terms of a localized MV structure. This suggestion is also consistent with the IR spectra of the monoamine compounds $[5]^{n+}$ (n = 0, 1) that show a clear shift of the ν(C≡C) band on oxidation to the monocationic species from 2103 to 2013 cm^{-1} (Figure 3b).

Table 2. Experimental and Calculated C≡C Stretching Frequencies/cm^{-1} for Complexes $[1-4]^{n+}$ (n = 0, 1, 2) and $[5]^{n+}$ (n = 0, 1)[a]

complex		0	+1	+2
1	exp.	2100 (s)	2018 (s)	2018 (s)
			2046 (sh)	2046 (sh)
			2070 (sh)	2070 (sh)
			2100 (s)	
	BLYP35	2119	2031 (92)	2043
			2098 (100)	
	B3LYP	2067	1994	2001
2	exp.	2100 (s)	2025 (s)	2025 (s)
			2046 (sh)	2046 (sh)
			2065 (sh)	2065 (sh)
			2100 (s)	2073 (s)
	BLYP35	2119	2048 (100)	2072
			2110 (19)	
3	exp.	2106 (s)	2024 (s)	2024 (s)
			2049 (sh)	2049 (sh)
			2079 (sh)	2079 (sh)
			2106 (s)	
	BLYP35	2131	2029 (100)	2043
			2111 (55)	
4	exp.	2106 (s)	2030 (s)	2030 (s)
			2050 (sh)	2050 (sh)
			2070 (sh)	2070 (sh)
			2106 (s)	
	BLYP35	2130	2050 (100)	2075
			2126 (8)	
5	exp.	2103 (w)	2013 (s)	
			2047 (sh)	
			2076 (sh)	
	BLYP35	2129	2021	

[a]Calculated IR frequencies were scaled by an empirical factor of 0.95.[58,59] Theoretical relative intensities/% for the monocationic forms in parentheses.

The UV−vis−NIR spectra of $[1-4]^{n+}$ (n = 0, 1, 2) and $[5]^{n+}$ (n = 0, 1) were collected using spectroelectrochemical methods from ca. 1 mM solutions in 0.1 M NBu_4PF_6/CH_2Cl_2, and data were corrected for the comproportionation equilibria.[60] Complexes **1**−**5** exhibit roughly the same overall electronic absorption pattern in the UV−vis−NIR region in their different oxidation states (Figure 4). The neutral complexes each feature two pronounced bands near 33 000 cm^{-1} and 25 000 cm^{-1}, arising from the two N→π* transitions commonly observed in triarylamine complexes of general form $NArAr'_2$.[40−42] No transitions are evident below 22 500 cm^{-1} in the electronic spectra of **1**−**5**.

Upon oxidation of **1**−**4** to $[1-4]^+$, a broad, low-intensity IVCT band near 6000 cm^{-1} and a distinct absorption band near 10 000 cm^{-1} appear in each case (Figure 4). However, the visible spectra of the tolyl systems **1** (Figures 4a,b) and **3** (Figures 4e,f) differ noticeably from those of the anisyl derivatives **2** (Figures 4c,d) and **4** (Figures 4g,h). Thus, while the spectra of **1** and **3** exhibit a series of unresolved transitions leading to a broad featureless absorption band envelope between 15 000 and 20 000

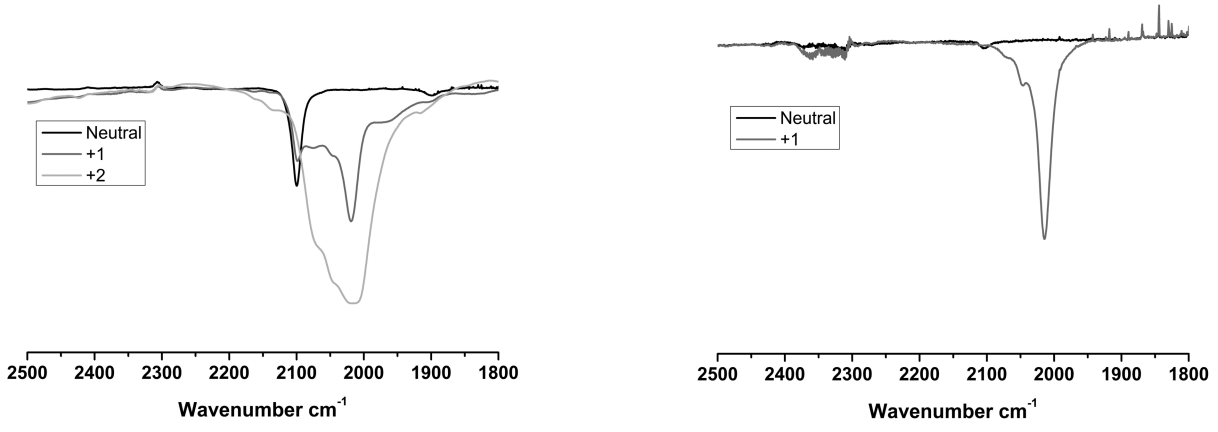

Figure 3. IR spectra of **1** (left) and **5** (right) showing the ν(C≡C) band in the various oxidation states generated by in situ electrochemical oxidation in CH_2Cl_2/0.1 M NBu_4PF_6 in an OTTLE cell.

dx.doi.org/10.1021/ic402538e | Inorg. Chem. 2014, 53, 1544−1554

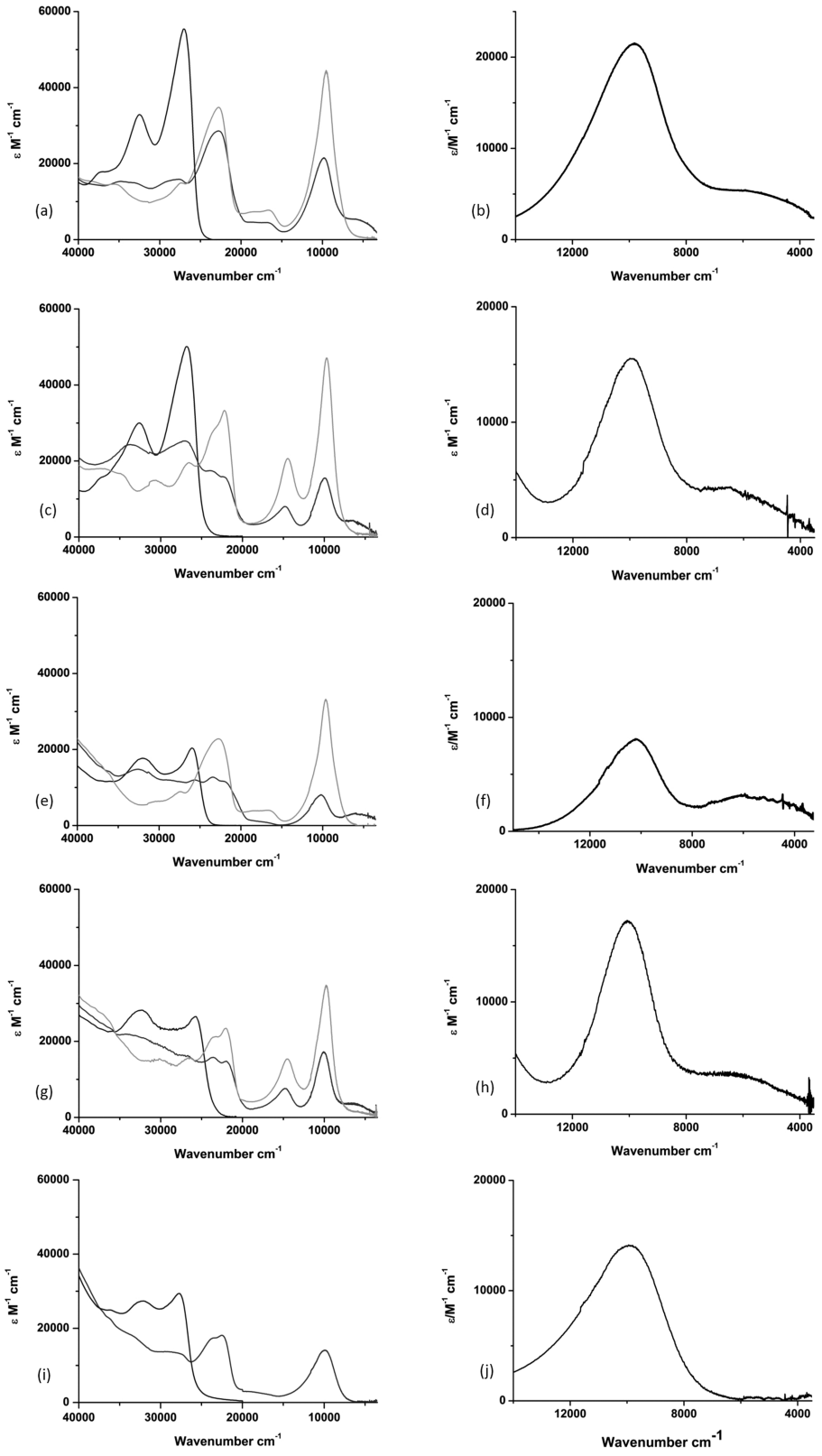

Figure 4. UV−vis−NIR spectra of compounds **1** (a), **2** (c), **3** (e), **4** (g), and **5** (i) in the various oxidation states generated by in situ electrochemical oxidation in CH_2Cl_2/0.1 M NBu_4PF_6 in an OTTLE cell. Expansions of the NIR region are given in (b), (d), (f), (h), and (j) for $[\mathbf{1}-\mathbf{5}]^+$, respectively.

cm^{-1}, for compounds **2** and **4** a much better-resolved band is apparent below 15000 cm^{-1} in each case (Figure 4), in addition to some unresolved bands at higher energy that are similar to those seen in the tolyl derivatives. For all complexes the two absorptions at 25 000 cm^{-1} and 33 000 cm^{-1} become less intense, and new features arise between 20 000 cm^{-1} and 25 000 cm^{-1} upon oxidation. This change in shape for the localized amine transitions is consistent with previous studies of the

dx.doi.org/10.1021/ic402538e | *Inorg. Chem.* 2014, 53, 1544−1554

Table 3. Calculated Ground State Properties for Complexes 1′−4′ and $[1'-4']^{2+}$[a]

	1′	1	2′	2[15]	3′	4′	$[1']^{2+}$	$[2']^{2+}$	$[3']^{2+}$	$[4']^{2+}$
μ_a/D	0.1		0.1		0.0	0.1	97.0	0.2	0.1	0.1
$\langle S^2\rangle$	0.0		0.0		0.0	0.0	1.1	1.1	1.1	1.1
d(N−C_6)/Å	1.411	1.423(7)	1.407	1.399(6)	1.413	1.408	1.380	1.395	1.377	1.392
	1.411		1.406		1.413	1.408	1.379	1.395	1.377	1.392
d(N−$C_{9/16}$)/Å	1.418	1.423(7)	1.420	1.442(6)	1.418	1.420	1.421	1.410	1.422	1.412
	1.419	1.409(8)	1.421	1.432(6)	1.418	1.420	1.421	1.410	1.422	1.412
d(C≡C)/Å	1.227	1.194(8)	1.227	1.171(7)	1.225	1.225	1.233	1.230	1.232	1.229
	1.227		1.227		1.225	1.225	1.233	1.230	1.232	1.229
d(Pt−C_1)/Å	2.028	1.999(6)	2.029	2.008(5)	2.029	2.029	2.010	2.016	2.011	2.015
	2.028		2.028		2.029	2.029	2.009	2.016	2.011	2.016
Ω/°[b]	6.4	6.2(1)	3.2	46.1(1)	11.5	24.8	6.5	12.6	−29.0	−29.3
	−1.1		−8.3		−10.7	−23.4	−11.0	−12.3	28.9	30.6
Θ/°[b]	44.6	50.2(3)	49.0	59.7(3)	44.4	−48.0	45.8	−42.0	−46.7	−42.7
	−44.9		−49.4		−44.4	48.2	−45.9	41.9	46.7	42.6

[a]Total dipole moment μ_a, spin expectation value $\langle S^2\rangle$ (theoretical value for singlet systems is 0.0), distance between nitrogen and the neighboring carbon atom of the bridge d(N−C_6), average distance between the two terminal phenyl rings and nitrogen d(N−$C_{9/16}$), C≡C bond length d(C≡C), platinum−carbon distances d(Pt−C_1), the average of dihedral angles ∠(P_1−Pt−C_3−C_4) and ∠(P_2−Pt−C_3−C_8) Ω, and the average of ∠(C_6−N−C_9−C_{10}) and ∠(C_6−N−C_{16}−C_{17}) Θ. Experimental data from the crystallographically determined structures of **1** and **2**[15] are included for comparison. [b]Magnitude of torsion is given by the absolute value; the opposite sign of the dihedral angles is due to the C_i-symmetric input structure of the optimization.

electronic spectra of triarylamine radical cations.[40−42,61,62] Upon further oxidation to the dicationic forms, the low-energy bands between 5000 and 7000 cm^{-1} collapse, supporting the IVCT assignment made here and elsewhere for $[\mathbf{2}]^+$,[15] and all the other absorptions below 25 000 cm^{-1} gain intensity (Figure 4). Oxidation of compound **5** (Figures 4i,j) gives rise to a spectrum that shows the changes of all the high-energy features of the spectra for $[\mathbf{1}-\mathbf{4}]^+$, with the absence of the lowest-energy transitions.

Quantum-Chemical Calculations and Electronic Spectroscopy. Previously, the electronic and spectroscopic properties of $[\mathbf{2}]^+$ were inferred from gas-phase calculations based on the crystallographic structure of **2**, reflecting the available computational capacity at the time.[15] To better understand the underlying electronic structure of these prototypical metal-bridged organic MV systems, we have also turned to quantum-chemical methods to study the complete series of complexes $[\mathbf{1}-\mathbf{4}]^{n+}$ (n = 0, 1, 2) and the mononuclear system $[\mathbf{5}]^{n+}$ (n = 0, 1), using the BLYP35 functional and the COSMO solvent model. Because of the high amount of exact exchange and the inclusion of a CH_2Cl_2 solvent model, this protocol is capable of describing the charge localization/delocalization behavior in the ground state for organic MV systems with reasonable accuracy, and the corresponding TDDFT calculations were found to be in good agreement with experimentally measured UV−vis−NIR spectral features. Indeed, this approach was developed and validated initially for the characterization of bis-triarylamine MV systems close to the Class II/III borderline[36,37] and thus should give a reliable description for the present systems as well. This provides an alternative to the simpler computational models employed previously.[15] Unrestricted structure optimization of $[\mathbf{1}'-\mathbf{4}']^{n+}$ (n = 0, 1, 2) and $[\mathbf{5}']^{n+}$ (n = 0, 1) gave stable minima evidenced by the absence of imaginary frequencies (the prime notation is used to distinguish the computational systems from the experimental complexes). For all neutral and dicationic complexes the singlet state gave the lowest energy. For the dications $[\mathbf{1}'-\mathbf{4}']^{2+}$ the spin expectation value $\langle S^2\rangle$ of 1.1 indicates a broken-symmetry (BS) description for a system with one antiferromagnetically coupled pair of spins. Indeed the singlet−triplet separation, which is calculated using the Yamaguchi spin projection procedure,[63,64] is only 1.8 kJ/mol for compound $[\mathbf{1}']^{2+}$, 0.8 kJ/mol for $[\mathbf{2}']^{2+}$, 2.4 kJ/mol for $[\mathbf{3}']^{2+}$, and 0.8 kJ/mol for $[\mathbf{4}']^{2+}$. The IR frequencies (e.g., $[\mathbf{1}']^{2+}$: ν(C≡C) = 2046 cm^{-1} for the triplet vs 2043 cm^{-1} for the singlet) and ground-state properties (e.g., $[\mathbf{1}']^{2+}$: d(N−C_6) = 1.383 for the triplet vs 1.380 for the BS singlet), which are discussed in this work, do not appreciably differ for the two spin states and thus only the singlet states are considered further. For the very important monocationic (MV) compounds, a doublet configuration is obtained, as expected, and calculations exhibit almost no spin contamination with the spin expectation values of 0.78 being only slightly larger than the theoretical value for doublet systems (0.75).

The neutral and dicationic structures $[\mathbf{1}-\mathbf{4}]^{n+}$ (n = 0, 2) are effectively symmetric, and some general trends can be observed across the series. In general the distances between the amine nitrogen atom and the first carbon atom of the bridge, d(N−C_6), are the most influenced by the oxidation state: they contract upon oxidation (Table 3; for atom labeling, see Figure 2). The d(N−C_6) distances are slightly longer for the neutral tolyl systems **1**′ and **3**′ (1.411 Å and 1.413 Å) than they are for the anisyl complexes **2**′ and **4**′ (1.407 Å and 1.408 Å), and the d(N−C_6) bond lengths are significantly shorter in the dicationic state for $[\mathbf{2}']^{2+}$ and $[\mathbf{4}']^{2+}$ by some 0.012−0.016 Å (1.395 Å and 1.392 Å) and shorter still for the tolyl derivatives $[\mathbf{1}']^{2+}$ and $[\mathbf{3}']^{2+}$ by 0.031−0.036 Å (1.380 Å and 1.377 Å). For **1**′, **2**′, **3**′, $[\mathbf{1}']^{2+}$, and $[\mathbf{2}']^{2+}$ the two phenyl rings of the bridge and the P−Pt−P axis are in plane, as the averaged dihedral angle Ω (average of ∠(P_1−Pt−C_3−C_4) and ∠(P_2−Pt−C_3−C_8)) reaches a maximum value of 12.6° for $[\mathbf{2}']^{2+}$. In general this torsion angle is larger (>23°) for complexes with triphenylphosphine ligands **4**′, $[\mathbf{3}']^{2+}$, and $[\mathbf{4}']^{2+}$, as expected, because of the increased steric interactions.

For the MV monocationic structures $[\mathbf{1}'-\mathbf{4}']^+$, minima with clearly localized electronic structures were obtained. In each case a significant asymmetry in the two halves of the molecule is observed, and the corresponding d(N−C_6) distances differ by at least 0.16 Å (Table 4), clearly pointing toward a localization of the redox event in $[\mathbf{1}'-\mathbf{4}']^+$ to one amine, consistent with the large calculated total dipole moment (>25 D; Table 4) in each

dx.doi.org/10.1021/ic402538e | Inorg. Chem. 2014, 53, 1544−1554

Table 4. Calculated Ground State Properties for Monocationic Complexes $[1'-4']^{+a}$

	$[1']^+$	$[2']^+$	$[3']^+$	$[4']^+$
μ_a/D	25.1	30.9	25.3	31.0
$\langle S^2\rangle$	0.78	0.78	0.78	0.78
d(N−C_6)/Å	1.403	1.401	1.405	1.404
	1.373	1.385	1.371	1.383
d(N−$C_{9/16}$)/Å	1.422	1.422	1.421	1.422
	1.426	1.416	1.427	1.417
d(C≡C)/Å	1.228	1.227	1.226	1.225
	1.238	1.234	1.237	1.233
d(Pt−C_1)/Å	2.017	2.021	2.017	2.021
	1.998	2.009	2.002	2.011
Ω/deg[b]	5.7	4.6	12.7	32.5
	−11.4	−7.0	−15.3	−29.5
Θ/deg[b]	48.8	51.7	47.8	50.7
	−50.1	−45.1	−50.7	−45.3

[a]Total dipole moment μ_a, spin expectation value $\langle S^2\rangle$ (theoretical value for doublet systems is 0.75), distance between nitrogen and the neighboring carbon atom of the bridge d(N−C_6), average distance between the two terminal phenyl rings and nitrogen d(N−$C_{9/16}$), C≡C bond length d(C≡C), the average of dihedral angles ∠(P_1−Pt−C_3−C_4) and ∠(P_2−Pt−C_3−C_8) Ω, and the average of ∠(C_6−N−C_9−C_{10}) and ∠(C_6−N−C_{16}−C_{17}) Θ. [b]Magnitude of torsion is given by the absolute value; the opposite sign of the dihedral angles is due to the C_i-symmetric input structure of the optimization.

case, and with the conclusions reached above on the basis of the IR data, and with the electronic spectroscopic data described by Jones et al.[15]

The localized behavior is further verified by the partial localization of the canonical orbitals and spin densities obtained for each of the compounds $[1'-4']^+$ (cf. Figure 5 and Supporting Information). The spin density is predominantly centered at one of the triarylamine units, with only a very small contribution from the platinum and supporting phosphine ligands. While calculations exhibit almost no spin contamination, the onset of spin polarization is observed: contrary to expectations a β-orbital (not shown in Figure 5) represents the occupied orbital with the highest energy ($[1']^+$: −5.55 eV; $[2']^+$: −5.39 eV; $[3']^+$: −5.50 eV; $[4']^+$: −5.34 eV). Taking the overlap as criterion this β orbital can be matched with the energetically highest-occupied α-orbital ($[1']^+$: −5.60 eV; $[2']^+$: −5.41 eV; $[3']^+$: −5.54 eV; $[4']^+$: −5.35 eV) to give the HOMO. The HOMO and SOMO are located on opposite halves of the complex (e.g., composition of the α-part $Ar_2C_6H_4C{\equiv}C/Pt(PEt_3)_2/C{\equiv}CC_6H_4N^+Ar_2$ for $[1]^+$: HOMO: 0/3/91%; SOMO: 67/9/13%) (Figure 5) and are similar in topology to the description in reference 15.

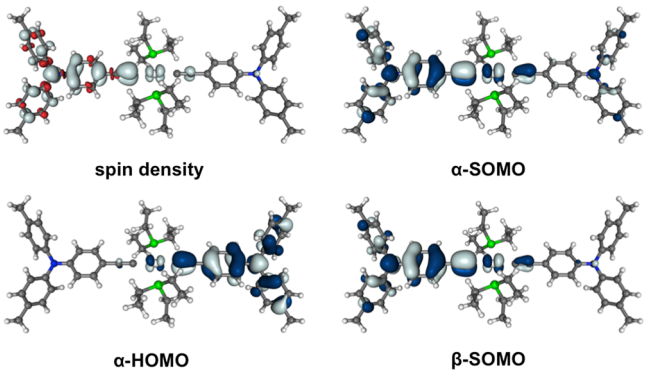

Figure 5. Spin density isosurface plot (top left, ± 0.002 au) and isosurface plots (± 0.03 au) of the α-SOMO (top right), α -HOMO (bottom left) and the β-SOMO (bottom right, virtual orbital) of $[1']^+$. Small differences in the α-SOMO and β-SOMO arise from spin polarization.

The subsequent vibrational frequency calculations show one ν(C≡C) band for the neutral and the dicationic complexes and two bands for the monocationic forms (Table 2). The frequencies obtained within a harmonic vibrational approach match the experimentally observed ones reasonably well after scaling by an empirical factor of 0.95,[58,59] although the calculations suggest a slightly larger intensity for the higher-energy band in $[1']^+$, in contrast to the experimental data. For all other cationic complexes, computations give the correct relative intensities. Full optimization using the commonly employed hybrid functional B3LYP leads to a delocalized Class III charge distribution for $[1']^+$ and thus to a single ν(C≡C) band at 1994 cm^{-1}. Note that the calculations do not reproduce the precise details of the splitting of the various ν(C≡C) bands, possibly due to neglect of Fermi coupling in the calculated results.

To gain more insight into the origin of the electronic transitions observed in the UV−vis−NIR spectroelectrochemical studies, and to both confirm the identity of the IVCT bands and test the accuracy of the computational methods, TDDFT calculations were performed for $[5']^+$ and the MV monocations $[1'-4']^+$ using the same basis sets, functionals, and solvent models (using nonequilibrium solvation as implemented in TURBOMOLE 6.4) as described above (Table 5). The results for $[1']^+$ and $[2']^+$ are illustrative for the entire series and will be discussed by way of example. The assignment of the broad low-energy NIR band of $[1']^+$ with its peak center around 5000 to 6000 cm^{-1} to an IVCT is straightforward on the basis of the quantum-chemical protocol. TDDFT calculations give the lowest excitation energy in $[1']^+$ at 5572 cm^{-1}, arising from the β-HOMO (231β) to β-SOMO (232β) transition (Figure 6). This transition has appreciable N→N^+ character, with significant contribution from the ethynyl parts of the bridge (Figure 6, Table 5). As might be expected from other studies reported elsewhere,[15,44] the mixing of platinum d-orbital character with the alkynyl π system in the ground state is relatively limited, and there is only a small contribution from the Pt d orbitals to the β-HOMO (2%) and β-SOMO (6%).

The TDDFT calculations also suggest that the intense asymmetric band envelope observed in the experimental spectrum of $[1]^+$ at around 10 000 cm^{-1} arises from two excitations, computed at 11 252 cm^{-1} and 12 046 cm^{-1} in $[1']^+$. The transition at 11 252 cm^{-1} is calculated to have substantial β-HOMO-1 (230β)→β-SOMO (69% contribution) and 228β→β-SOMO (12% contribution) character. The β-HOMO-1 and the 228β orbital are both unevenly distributed over the molecular backbone (Figure 6), and while the β-HOMO-1 exhibits noticeable Pt(d)/C≡C (13/26%) character, there is substantially less d-orbital character (2%) in 228β. Thus the transition at 11 252 cm^{-1} also exhibits CT character and is best described as a π→N^+ excitation, with considerably more bridge character in the donor orbital than for the IVCT transition at 5572 cm^{-1}. The transition at 12 046 cm^{-1} arises from transitions between 227β (41% contribution) and 229β (34% contribution) and the β-SOMO. Both orbitals are mainly localized in the metal coordination sphere (50% and 24%) and the ethynyl parts of the bridge (34% and 67%), giving this transition significant MLCT (Pt→N^+) character. Four low-intensity excitations are computed for $[1']^+$ between 15 000 and 20 000 cm^{-1}, consistent

dx.doi.org/10.1021/ic402538e | Inorg. Chem. 2014, 53, 1544−1554

Table 5. Calculated Excited-State Parameters for $[1']^+$ and $[2']^+$[a]

number	$[1']^+$		$[2']^+$	
	E_{trans}/cm^{-1} (μ_t/D)	character	E_{trans}/cm^{-1} (μ_t/D)	character
1	5572 (15.3)	$N \rightarrow N^+$ intervalence CT	5628 (13.0)	$N \rightarrow N^+$ intervalence CT
2	11 252 (6.6)	$\pi \rightarrow N^+$ bridge to amine CT	11 062 (8.2)	$\pi \rightarrow N^+$ bridge to amine CT
3	12 046 (4.0)	$Pt^+ \rightarrow N^+$ metal to amine ligand CT	13 588 (1.2)	$Pt^+ \rightarrow N^+$ metal to amine ligand CT
4	15 790 (1.0)	$Pt^+ \rightarrow N^+$ metal to amine ligand CT	16 000 (1.6)	$\pi \rightarrow N^+$ bridge to amine CT
5	16 162 (1.3)	$\pi \rightarrow N^+$ bridge to amine ligand CT	16 529 (4.9)	intraligand transition at triarylamine
6	17 548 (0.2)	$Pt^+ \rightarrow N^+$ metal to amine ligand CT	17 108 (0.2)	$Pt^+ \rightarrow N^+$ metal to amine ligand CT
7	19 679 (1.7)	intraligand transition at triarylamine	19 112 (0.2)	$Pt^+ \rightarrow N^+$ metal to amine ligand CT

[a]UV–vis–NIR transition energies E_{trans}/cm^{-1}, transition dipole moments μ_t/D, and character of the excitation.

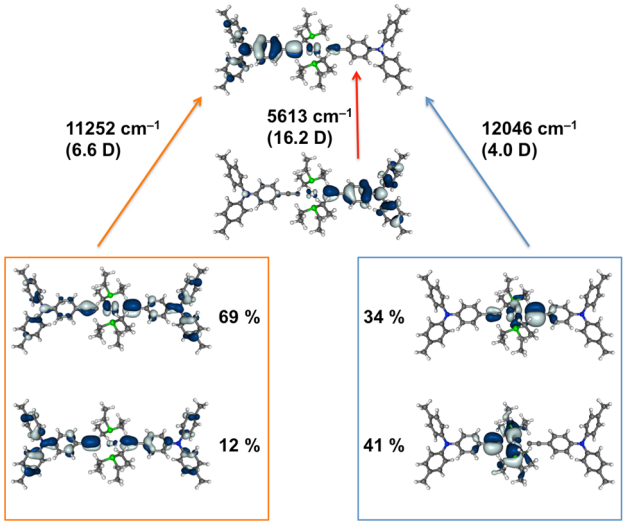

Figure 6. Isosurface plots (± 0.03 au) of the orbitals involved in the first three UV–vis–NIR transitions for monocationic radical $[1']^+$; transition energies and transition dipole moments are given in parentheses.

with the observation of multiple transitions in this range (Figure 4). The calculated transitions at 15 790 cm^{-1} (μ_t = 1.0 D) and 17 548 cm^{-1} (μ_t = 0.2 D) also have significant MLCT character, while the excitation at 16 162 cm^{-1} (μ_t = 1.3 D) corresponds to a $\pi \rightarrow N^+$ transition. The highest energy calculated excitation at 19 679 cm^{-1} (μ_t = 1.7 D) can be attributed to an intraligand transition associated with the oxidized triarylamine moiety (see Supporting Information).

On the basis of the computed transition dipole moments, the calculations appear to overestimate the relative intensity of the IVCT band significantly. (In fact, the computed transition dipole moment of 15.3 D is larger than the sum of those for the second (μ_t = 6.6 D) and third (μ_t = 4.0 D) transitions, while the experimentally observed IVCT band at 5000 to 6000 cm^{-1} exhibits much lower intensity than the band envelope near 10000 cm^{-1}.) The low intensity and the broadening of the IVCT band in Class II systems is well-known to be caused by vibronic coupling.[4,13] The computations do not take into account and may thus not be expected to reproduce the relative intensities faithfully.

The first three transitions of $[2']^+$ exhibit very similar character to that of the tolyl analogue $[1']^+$. Interestingly, the calculated "IVCT" transition in $[2']^+$ at 5628 cm^{-1} (μ_t = 13.0 D) is blue-shifted by only 56 cm^{-1} relative to the analogous transition in $[1']^+$ (Table 5). The quantum-chemical treatment thus suggests a less-pronounced influence of the methoxy groups on the IVCT band than is found experimentally (Figure 4). The BLYP35/COSMO combination has been found to moderately but systematically underestimate the IVCT excitation energies for related organic Class II mixed valence radical cations.[36,37] It is conceivable that this underestimation will be more pronounced in excitations with greater "true" charge-transfer character. In comparison to that of compound $[1']^+$, the second ($\pi \rightarrow N^+$) transition of $[2']^+$ is red-shifted by 190 cm^{-1}, while the calculated third (MLCT) transition for $[2']^+$ is some 1500 cm^{-1} higher in energy and of lower intensity than it is for $[1']^+$. This compares well with the experimental observations (Figure 4) with $[1]^+$ featuring the band envelope at 9750 cm^{-1}, while in $[2]^+$ comparable features are observed near 9950 cm^{-1} (Table 5).

Also consistent with experimental observation, the computed transitions between 15 000 and 20 000 cm^{-1} change appreciably when going from tolyl ($[1']^+$) to anisyl ($[2']^+$) substituents on the amine moieties (Table 5). The experimental data for $[2]^+$ in this region is dominated by an intense band centered at 14 500 cm^{-1}, which compares with a less-intense broad band in $[1]^+$ between 14 000 and 20 000 cm^{-1}. The TDDFT calculations for $[2']^+$ feature two excitations of similar energy at 16 000 cm^{-1} and 16 529 cm^{-1}. While the first exhibits a relatively low-transition dipole moment (μ_t = 1.6 D), the second is more intense (μ_t = 4.9 D) and thus is likely the major contributor to the experimentally observed absorption band. However, the character of these two transitions differs appreciably. The lower-energy, lower-intensity excitation at 16 000 cm^{-1} originates from delocalized orbitals (244β and 246β) and goes to the β-SOMO (248β). It thus is best described in terms of a $\pi \rightarrow N^+$ transition (Table 5). The higher-energy, more-intense excitation at 16 529 cm^{-1} originates essentially from a single orbital, which is distributed over the same $Ar_2NC_6H_4C{\equiv}C$ moiety (94%) as the β-SOMO. The excitation thus exhibits no CT character and is better described as a localized transition arising from the amine radical cation (Table

dx.doi.org/10.1021/ic402538e | Inorg. Chem. 2014, 53, 1544–1554

Table 6. Calculated Excited State Parameters for $[3'-5']^{+a}$

$[3']^+$		$[4']^+$		$[5']^+$	
E_{trans}/cm^{-1} (μ_t/D)	character	E_{trans}/cm^{-1} (μ_t/D)	character	E_{trans}/cm^{-1} (μ_t/D)	character
5716 (13.8)	N→N^+ IVCT	5626 (11.0)	N→N^+ IVCT	10 543 (7.0)	π-tolyl→N^+ CT
11 295 (5.5)	mixed π→N^+ and Pt^+→N^+ MLCT	10 928 (8.8)	mixed π→N^+ and Pt^+→N^+ MLCT	11 532 (8.7)	intraligand transition at triarylamine
11 960 (5.8)	mixed π→N^+ and Pt^+→N^+ MLCT	12 798 (2.5)	mixed π→N^+ and Pt^+→N^+ MLCT	13 892 (1.9)	mixed π-tolyl→N^+ and Pt^+→N^+ MLCT

[a] UV−vis−NIR transition energies E_{trans}/cm^{-1}, transition dipole moments μ_t/D, and character for the first three excitations.

6). The TDDFT calculations also predict three more low-intensity excitations at 17 108, 19 112, and 19 562 cm^{-1} ($\mu_t \leq 0.6$ D), which are unlikely to have a significant role in determining the overall appearance of the absorption spectrum.

Turning attention briefly to the triphenylphosphine complex $[3]^+$, a small blue shift for the two lowest-energy absorption bands is observed in the experimental spectrum relative to those in the PEt_3 analogue $[1]^+$ (Figure 4f). This trend is reproduced in the TDDFT calculations with the computational models $[3']^+$ and $[1']^+$ (Tables 5 and 6) and likely reflects the lower electron-donating ability of the PPh_3 ligand, which consequently lowers the energy of the various donor orbitals. The most obvious difference in the TDDFT results from $[3']^+$ relative to $[1']^+$ is the character of the calculated transition at 11 295 cm^{-1} (5.5 D), which is of mixed π→N^+ and MLCT character for $[3']^+$. The IVCT excitation calculated at 5716 cm^{-1} in $[3']^+$ is at almost the same energy as that calculated for the PEt_3 derivative $[1']^+$, and the limited influence of the phosphine substituents on the IVCT band is a further indication of the limited role the metal center plays in this transition. The largest energy shift between $[1']^+$ and $[3']^+$ can be observed for the third transition (11 960 cm^{-1}), which is due to the coupling of π→N^+-type and MLCT transitions for the associated band. Similarly, the character of the transitions for $[4']^+$ (e.g., 5626 cm^{-1}, μ_t = 11.0 D) are nearly unchanged compared to $[2']^+$.

As expected, TDDFT calculations from the monocation $[5']^+$ do not exhibit any transitions below 10 000 cm^{-1}. The absorption pattern above 10 000 cm^{-1} exhibits the same features as $[3']^+$. The first excitation of $[5']^+$ is calculated at 10 543 cm^{-1}, which is red-shifted by about 700 cm^{-1} compared to $[3']^+$ (11 295 cm^{-1}). This can be explained by the nature of the involved orbital. For $[3']^+$ this transition occurs from a delocalized orbital, which has significant contributions from the second triarylamine group (Supporting Information, Tables S5 and S6). As this group is absent in $[5']^+$, the orbital is destabilized (−6.41 eV compared to −6.60 eV for $[3']^+$) in the ground state and is predominantly localized at the tolyl ligand (78%) (Supporting Information, Tables S9 and S10).

CONCLUSIONS

This combined spectroscopic and computational study demonstrates that the nature of the UV−vis−NIR transitions observed upon oxidation of the platinum-bridged bis-triarylamine compounds **1**−**4** are consistent across the series and that the effect of the phosphine ligand on most of them is relatively insignificant. These transitions have been accurately modeled using a computational protocol based on the BLYP35 functional and a suitable solvent model, allowing a more detailed investigation than was possible a few years ago. As expected for localized MV systems, the lowest-energy transition at around 5600 cm^{-1} corresponds to an IVCT excitation for all bis-triarylamine complexes $[1-4]^+$. Generally the agreement between computed and experimentally observed IVCT excitation energies is better for the tolyl complexes $[1]^+$ and $[3]^+$ than it is for the anisyl-substituted compounds $[2]^+$ and $[4]^+$. While the assignment of the second excitation to a CT transition from a delocalized π orbital and of the third to a CT from the platinum moiety to the cationic triarylamine unit is straightforward for $[1]^+$ and $[2]^+$, those excitations start to mix for the triphenylphosphine complexes $[3]^+$ and $[4]^+$. For complex $[5]^+$ no IVCT transition is observed due to the absence of the second triarylamine unit. Here the first excitation corresponds to a CT transition from a π orbital, which is mainly tolyl-centered, to the cationic triarylamine unit.

The ability of computational methods based on appropriately balanced hybrid functionals to successfully model, and hence predict, the optoelectronic properties of even relatively large and complex molecular materials promises much not only for the interpretation of experimental data, but also for computational screening and molecular design optimization in advance of synthetic effort, expenditure of chemical resources, and waste generation. When used sensibly, the predictive power of DFT methods may now be seen as a viable tool alongside experimental molecular design and feedback-driven optimization as a route to molecular materials with designed optoelectronic properties.

EXPERIMENTAL SECTION

Computational Details. Full structure optimizations and analysis of all ground-state properties were performed using a locally modified version of the TURBOMOLE 6.4[65] program code enabling the use of the BLYP35 hybrid functional based on

$$E_{XC} = 0.65(E_X^{LSDA} + \Delta E_X^{B88}) + 0.35E_X^{exact} + E_C^{LYP}$$

which proved to give accurate results for organic MV systems.[36,37,66−68] For comparison with previous studies,[15] results obtained using the B3LYP functional were considered in selected cases.[69] Split-valence def2-SVP basis sets were employed on all lighter atoms, together with the corresponding def2-SVP effective-core potential and a corresponding valence basis set for platinum.[70−72] For molecules **1**−**4** C_i-symmetric structures were used as starting points for optimizations, and no constraints were employed. Computed harmonic vibrational frequencies were scaled by an empirical factor of 0.95.[58,59] To account for solvent effects, the conductor-like-screening (COSMO) solvent model was employed for ground state structure optimizations and analysis as well as in subsequent TDDFT calculations of excitation energies and transition dipole moments in TURBOMOLE.[73] Dichloromethane (ε = 8.93) was used, as experimental data were collected in this solvent (nonequilibrium solvation was assumed in the TDDFT calculations). Spin density and molecular orbital isosurface plots were generated with the Molekel program.[74]

dx.doi.org/10.1021/ic402538e | Inorg. Chem. 2014, 53, 1544−1554

Crystal Data for **1**. $C_{56}H_{66}N_2P_2Pt$, M = 1024.14, triclinic, space group $P\bar{1}$, a = 9.9533(5), b = 11.0652(7), c = 11.5908(7) Å, α = 76.561(5), β = 88.071(4), γ = 85.292(5)°, U = 1237.3(1) Å^3, $F(000)$ = 524, Z = 1, D_c = 1.374 g m^{-3}, μ = 2.937 mm^{-1}, T = 120(1) K. 19 690 reflections ($2.69 \leq \theta \leq 29.5°$) were collected on an Agilent Gemini S-Ultra diffractometer (graphite monochromator, λ Mo Kα, λ = 0.71073 Å, ω scan, 1°/frame) equipped with a Cryostream (Oxford Cryosystems) open-flow nitrogen cryostat, yielding 6893 unique reflections (R_{merg} = 0.0436). The structure was solved by direct methods and refined by full-matrix least-squares on F^2 for all data using SHELXTL and OLEX2 software.[75,76] All nondisordered non-hydrogen atoms were refined with anisotropic displacement parameters; disordered atoms of Et groups were refined isotropically with fixed SOF = 0.5. H-atoms were located on the difference map and refined isotropically except the H-atoms of disordered groups, which were placed in calculated positions and refined in "riding" mode. Final w$R_2(F^2)$ = 0.0636 for all data (349 refined parameters), conventional $R(F)$ = 0.0292 for 6696 reflections with $I \geq 2\sigma$, GOF = 1.013.

■ ASSOCIATED CONTENT

Supporting Information

Full details of the syntheses and characterization of 4-ethynylenephenylenedi-*p*-tolylamine and compounds **1**−**5**. Figures showing the IR spectra of $[\mathbf{1}]^{n+}$, $[\mathbf{2}]^{n+}$, and $[\mathbf{4}]^{n+}$ (n = 0, 1, 2). Figures showing the UV−vis−NIR spectra of $[\mathbf{1}-\mathbf{4}]^{n+}$ (n = 0, 1, 2) and $[\mathbf{5}]^{n+}$ (n = 0, 1). Tables of orbital energies, orbital composition, and calculated excited-state parameters for $[\mathbf{1}'-\mathbf{5}']^+$. Plots of the spin density isosurfaces of $[\mathbf{1}'-\mathbf{5}']^+$. Plots of the orbitals involved in the first 10 electronic transitions of $[\mathbf{1}']^+$ and $[\mathbf{2}']^+$. Plots of the orbitals involved in the first five electronic transitions of $[\mathbf{3}']^+$ and $[\mathbf{4}']^+$. Plots of the β-HOMO and β-SOMO of $[\mathbf{5}']^+$. This material is available free of charge via the Internet at http://pubs.acs.org. Crystallographic data for the structure have been deposited with the Cambridge Crystallographic Data Centre as supplementary publication CCDC-961163.

■ AUTHOR INFORMATION

Corresponding Author

*E-mail: martin.kaupp@tu-berlin.de (M.K.), paul.low@uwa.edu.au (P.J.L.).

Notes

The authors declare no competing financial interest.

■ ACKNOWLEDGMENTS

This work has been supported by the Berlin DFG cluster of excellence on "Unifying Concepts in Catalysis" (UniCat), by DFG project KA1187/13-1, and by the Engineering and Physical Sciences Research Council (EPSRC). M.P. is grateful to UniCat, the Berlin International Graduate School of Natural Sciences and Engineering (BIG-NSE), and the German Academic Exchange Service (DAAD) for funding. P.J.L. held an EPSRC Leadership Fellowship, and gratefully acknowledges funding from the ARC in the form of a Future Fellowship (FTFT120100073). K.B.V. gratefully acknowledges funding for Ph.D. studies from the EPSRC. Dr. Hilke Bahmann is gratefully acknowledged for modifying the TURBOMOLE 6.4 code.

■ REFERENCES

(1) Sakamoto, R.; Kume, S.; Nishihara, H. *Chem.—Eur. J.* **2008**, *14*, 6978.

(2) (a) Low, P. J. *Dalton Trans.* **2005**, 2821. (b) Rigaut, S. *Dalton Trans.* **2013**, *42*, 15859. (c) Launay, J. P. *Coord. Chem. Rev.* **2013**, *257*, 1544. (d) Sakamoto, R.; Katagiri, S.; Maeda, H.; Nishihara, H. *Coord. Chem. Rev.* **2013**, *257*, 1493. (e) Haga, M.; Kobayashi, K.; Terada, K. *Coord. Chem. Rev.* **2007**, *251*, 2688.

(3) (a) Hush, N. S. *Electrochim. Acta* **1968**, *13*, 1005. (b) Hush, N. S. *Coord. Chem. Rev.* **1985**, *64*, 135. (c) Creutz, C. *Prog. Inorg. Chem.* **1983**, *30*, 1.

(4) Brunschwig, B. S.; Creutz, C.; Sutin, N. *Chem. Soc. Rev.* **2002**, *31*, 168.

(5) Demadis, K. D.; Hartshorn, C. M.; Meyer, T. J. *Chem. Rev.* **2001**, *101*, 2655.

(6) Low, P.; Brown, N. *J. Cluster Sci.* **2010**, *21*, 235.

(7) Richardson, D. E.; Taube, H. *Coord. Chem. Rev.* **1984**, *60*, 107.

(8) Launay, J. P. *Chem. Soc. Rev.* **2001**, *30*, 386.

(9) Kaim, W.; Sarkar, B.; Lahiri, G. K. *Mixed-Valence Intermediates as Ideal Targets for Spectroelectrochemistry (SEC);* RSC Publishing: Cambridge, 2008.

(10) Kaim, W.; Klein, A.; Glockle, M. *Acc. Chem. Res.* **2000**, *33*, 755.

(11) Creutz, C.; Taube, H. *J. Am. Chem. Soc.* **1973**, *95*, 1086.

(12) Creutz, C.; Taube, H. *J. Am. Chem. Soc.* **1969**, *91*, 3988.

(13) Heckmann, A.; Lambert, C. *Angew. Chem., Int. Ed.* **2012**, *51*, 326.

(14) Liddle, B. J.; Wanniarachchi, S.; Hewage, J. S.; Lindeman, S. V.; Bennett, B.; Gardinier, J. R. *Inorg. Chem.* **2012**, *51*, 12720.

(15) Jones, S. C.; Coropceanu, V.; Barlow, S.; Kinnibrugh, T.; Timofeeva, T.; Bredas, J.-L.; Marder, S. R. *J. Am. Chem. Soc.* **2004**, *126*, 11782.

(16) Vacher, A.; Barriere, F.; Camerel, F.; Bergamini, J.-F.; Roisnel, T.; Lorcy, D. *Dalton Trans.* **2013**, *42*, 383.

(17) Vacher, A.; Barriere, F.; Roisnel, T.; Piekara-Sady, L.; Lorcy, D. *Organometallics* **2011**, *30*, 3570.

(18) Cai, X.-M.; Zhang, X.-Y.; Savchenko, J.; Cao, Z.; Ren, T.; Zuo, J.-L. *Organometallics* **2012**, *31*, 8591.

(19) Bushby, R. J.; Kilner, C.; Taylor, N.; Williams, R. A. *Polyhedron* **2008**, *27*, 383.

(20) Meng, F.; Hervault, Y.-M.; Norel, L.; Costuas, K.; Van Dyck, C.; Geskin, V.; Cornil, J.; Hng, H. H.; Rigaut, S.; Chen, X. *Chem. Sci.* **2012**, *3*, 3113.

(21) Luo, L.; Benameur, A.; Brignou, P.; Choi, S. H.; Rigaut, S.; Frisbie, C. D. *J. Phys. Chem. C* **2011**, *115*, 19955.

(22) Kim, B.; Beebe, J. M.; Olivier, C.; Rigaut, S.; Touchard, D.; Kushmerick, J. G.; Zhu, X. Y.; Frisbie, C. D. *J. Phys. Chem. C* **2007**, *111*, 7521.

(23) Mahapatro, A. K.; Ying, J.; Ren, T.; Janes, D. B. *Nano Lett.* **2008**, *8*, 2131.

(24) Liu, K.; Li, G.; Wang, X.; Wang, F. *J. Phys. Chem. C* **2008**, *112*, 4342.

(25) Liu, K.; Wang, X.; Wang, F. *ACS Nano* **2008**, *2*, 2315.

(26) Marques-Gonzalez, S.; Yufit, D. S.; Howard, J. A. K.; Martin, S.; Osorio, H. M.; Garcia-Suarez, V. M.; Nichols, R. J.; Higgins, S. J.; Cea, P.; Low, P. J. *Dalton Trans.* **2013**, *42*, 338.

(27) D'Alessandro, D. M.; Keene, F. R. *Chem. Soc. Rev.* **2006**, *35*, 424.

(28) Lear, B. J.; Chisholm, M. H. *Inorg. Chem.* **2009**, *48*, 10954.

(29) Dattelbaum, D. M.; Hartshorn, C. M.; Meyer, T. J. *J. Am. Chem. Soc.* **2002**, *124*, 4938.

(30) Creutz, C.; Newton, M. D.; Sutin, N. *J. Photochem. Photobiol., A.* **1994**, *82*, 47.

(31) Aguirre-Etcheverry, P.; O'Hare, D. *Chem. Rev.* **2010**, *110*, 4839.

(32) Robin, M. B.; Day, P. *Adv. Inorg. Chem. Radiochem.* **1967**, *10*, 247.

(33) Hush, N. S. *Prog. Inorg. Chem.* **1967**, *8*, 391.

(34) Brown, N. J.; Lancashire, H. N.; Fox, M. A.; Collison, D.; Edge, R.; Yufit, D. S.; Howard, J. A. K.; Whiteley, M. W.; Low, P. J. *Organometallics* **2011**, *30*, 884.

(35) Fox, M. A.; Roberts, R. L.; Baines, T. E.; Le Guennic, B.; Halet, J.-F.; Hartl, F.; Yufit, D. S.; Albesa-Jové, D.; Howard, J. A. K.; Low, P. J. *J. Am. Chem. Soc.* **2008**, *130*, 3566.

(36) Renz, M.; Theilacker, K.; Lambert, C.; Kaupp, M. *J. Am. Chem. Soc.* **2009**, *131*, 16292.

(37) Kaupp, M.; Renz, M.; Parthey, M.; Stolte, M.; Würthner, F.; Lambert, C. *Phys. Chem. Chem. Phys.* **2011**, *13*, 16973.

(38) (a) Parthey, M.; Gluyas, J. B. G.; Schauer, P. A.; Yufit, D. S.; Howard, J. A. K.; Kaupp, M.; Low, P. J. *Chem.—Eur. J.* **2013**, *19*, 9780.

(b) Vincent, K. B.; Zeng, Q.; Parthey, M.; Yufit, D. S.; Howard, J. A. K.; Hartl, F.; Kaupp, M.; Low, P. J. *Organometallics* **2013**, *32*, 6022.
(39) Sonogashira, K.; Yatake, T.; Tohda, Y.; Takahashi, S.; Hagihara, N. J. *J. Chem. Soc., Chem. Commun.* **1977**, 291.
(40) Low, P. J.; Paterson, M. A. J.; Goeta, A. E.; Yufit, D. S.; Howard, J. A. K.; Cherryman, J. C.; Tackley, D. R.; Brown, B. *J. Mater. Chem.* **2004**, *14*, 2516.
(41) Low, P. J.; Paterson, M. A. J.; Puschmann, H.; Goeta, A. E.; Howard, J. A. K.; Lambert, C.; Cherryman, J. C.; Tackley, D. R.; Leeming, S.; Brown, B. *Chem.—Eur. J.* **2004**, *10*, 83.
(42) Low, P. J.; Paterson, M. A. J.; Yufit, D. S.; Howard, J. A. K.; Cherryman, J. C.; Tackley, D. R.; Brook, R.; Brown, B. *J. Mater. Chem.* **2005**, *15*, 2304.
(43) Carpenter, J. P.; Lukehart, C. M. *Inorg. Chim. Acta* **1991**, *190*, 7.
(44) Mayor, M.; von Hanisch, C.; Weber, H. B.; Reichert, J.; Beckmann, D. *Angew. Chem., Int. Ed.* **2002**, *41*, 1183.
(45) Gagnon, K.; Aly, S. M.; Brisach-Wittmeyer, A.; Bellows, D.; Berube, J.-F.; Caron, L.; Abd-El-Aziz, A. S.; Fortin, D.; Harvey, P. D. *Organometallics* **2008**, *27*, 2201.
(46) Adams, C. J.; Bowen, L. E. *Dalton Trans.* **2005**, 2239.
(47) Leininger, S.; Stang, P. J.; Huang, S. P. *Organometallics* **1998**, *17*, 3981.
(48) Minh-Hai, N.; Yip, J. H. K. *Organometallics* **2011**, *30*, 6383.
(49) Zhou, G.; Wong, W.-Y.; Poon, S.-Y.; Ye, C.; Lin, Z. *Adv. Funct. Mater.* **2009**, *19*, 531.
(50) Evans, D. H. *Chem. Rev.* **2008**, *108*, 2113.
(51) D'Alessandro, D. M.; Keene, F. R. *Dalton Trans.* **2004**, 3950.
(52) Barriere, F.; Camire, N.; Geiger, W. E.; Mueller-Westerhoff, U. T.; Sanders, R. *J. Am. Chem. Soc.* **2002**, *124*, 7262.
(53) Barriere, F.; Geiger, W. E. *J. Am. Chem. Soc.* **2006**, *128*, 3980.
(54) Richardson, D. E.; Taube, H. *Inorg. Chem.* **1981**, *20*, 1278.
(55) Lambert, C.; Nöll, G. *J. Am. Chem. Soc.* **1999**, *121*, 8434.
(56) Kaim, W.; Klein, A. *Spectroelectrochemistry*; RSC Publishing: Cambridge, 2008.
(57) Denis, R.; Toupet, L.; Paul, F.; Lapinte, C. *Organometallics* **2000**, *19*, 4240.
(58) Scott, A. P.; Radom, L. *J. Phys. Chem.* **1996**, *100*, 16502.
(59) Roder, J. C.; Meyer, F.; Hyla-Kryspin, I.; Winter, R. F.; Kaifer, E. *Chem.—Eur. J.* **2003**, *9*, 2636.
(60) (a) Richardson, D. E.; Taube, H. *Coord. Chem. Rev.* **1984**, *60*, 107. (b) Arnold, D. P.; Heath, G. A.; James, D. A. *J. Porphyrins Phthalocyanines* **1999**, *3*, S. (c) Barrière, F.; Camire, N.; Geiger, W. E.; Mueller-Westerhoff, U. T.; Sanders, R. *J. Am. Chem. Soc.* **2002**, *124*, 7262.
(61) Amthor, S.; Noller, B.; Lambert, C. *Chem. Phys.* **2005**, *316*, 141.
(62) Barlow, S.; Risko, C.; Chung, S.-J.; Tucker, N. M.; Coropceanu, V.; Jones, S. C.; Levi, Z.; Bredas, J.-L.; Marder, S. R. *J. Am. Chem. Soc.* **2005**, *127*, 16900.
(63) Shoji, M.; Koizumi, K.; Kitagawa, Y.; Kawakami, T.; Yamanaka, S.; Okumura, M.; Yamaguchi, K. *Chem. Phys. Lett.* **2006**, *432*, 343.
(64) Soda, T.; Kitagawa, Y.; Onishi, T.; Takano, Y.; Shigeta, Y.; Nagao, H.; Yoshioka, Y.; Yamaguchi, K. *Chem. Phys. Lett.* **2000**, *319*, 223.
(65) *TURBOMOLE V6.4;* Turbomole GmbH: Karlsruhe, Germany, 2012.
(66) Völker, S. F.; Renz, M.; Kaupp, M.; Lambert, C. *Chem.—Eur. J.* **2011**, *17*, 14147.
(67) Renz, M.; Kaupp, M. *J. Phys. Chem. A* **2012**, *116*, 10629.
(68) Renz, M.; Kess, M.; Diedenhofen, M.; Klamt, A.; Kaupp, M. *J. Chem. Theory Comput.* **2012**, *8*, 4189.
(69) Stephens, P. J.; Devlin, J. F.; Chabalowski, C. F.; Frisch, M. J. *J. Phys. Chem.* **1994**, *98*, 11623.
(70) Weigend, F.; Ahlrichs, R. *Phys. Chem. Chem. Phys.* **2005**, *7*, 3297.
(71) Schäfer, A.; Horn, H.; Ahlrichs, R. *J. Chem. Phys.* **1992**, *97*, 2571.
(72) Andrae, D.; Häussermann, U.; Dolg, M.; Stoll, H.; Preuss, H. *Theor. Chim. Acta* **1990**, *77*, 123.
(73) Klamt, A.; Schüürmann, G. *J. Chem. Soc., Perkin Trans. 2* **1993**, *5*, 799.
(74) Varetto, U., *MOLEKEL 5.4;* Swiss National Supercomputing Centre: Manno, Switzerland, 2009.
(75) Sheldrick, G. M. *Acta Crystallogr., Sect. A* **2008**, *64*, 112.
(76) Dolomanov, O. V.; Bourhis, L. J.; Gildea, R. J.; Howard, J. A. K.; Puschmann, H. *J. Appl. Crystallogr.* **2009**, *42*, 339.